Legacy Atmospheric Profiles and Derived Products From GOES-16: Validation and Applications

Timothy J. Schmit[1] , Jun Li[2] , Su Jeong Lee[2,3], Zhenglong Li[2] , Richard Dworak[2], Yong-Keun Lee[4] , Michael Bowlan[5] , Jordan Gerth[2] , Graeme D. Martin[2], William Straka[2] , Kevin C. Baggett[2], and Lee Cronce[2]

[1]NOAA/NESDIS Center for Satellite Applications and Research Advanced Satellite Products Branch, Madison, WI, USA, [2]Cooperative Institute for Meteorological Satellite Studies (CIMSS), University of Wisconsin-Madison, Madison, WI, USA, [3]Atmospheric Science and Engineering Department, Ewha Womans University, Seoul, South Korea, [4]CMNS-Earth System Science Interdisciplinary Center, University of Maryland, College Park, MD, USA, [5]Cooperative Institute for Mesoscale Meteorological Studies (CIMMS), University of Oklahoma, Norman, OK, USA

Abstract The Geostationary Operational Environmental Satellite-R (GOES-R) series started a new era for the U.S. geostationary satellite observing system. The Advanced Baseline Imager (ABI) onboard the GOES-R series has fine temporal (30 s to 10 min) and spatial resolutions (0.5–2 km), and 16 spectral bands. However, due to the lack of an infrared sounder, the ABI is used to continue the legacy atmospheric profile (LAP) products that the previous GOES Sounder has, including the legacy atmospheric moisture profile, legacy atmospheric temperature profile, total precipitable water, layered precipitable water, and derived atmospheric stability indices. The ABI LAP retrieval algorithms have been developed under the GOES-R series Algorithm Working Group (AWG) program funded by the GOES-R Program Office. The LAP products from GOES-16 have been operational and validated with a series of reference data sets including radiosonde observations, the Global Positioning System from SuomiNet, the Advanced Microwave Scanning Radiometer 2 total precipitable water measurements, as well as global operational analysis from National Oceanic and Atmospheric Administration and European Centre for Medium-Range Weather Forecasts models, for almost a year (from 2017 to 2018) to assure the data quality for applications. In addition, the LAP products have been successfully demonstrated at the Hazardous Weather Testbed experiments in the summer of 2017 and the spring of 2018. Both validation results and Hazardous Weather Testbed demonstrations indicate that the GOES-R series LAP products meet the product requirements and provide added value over NWP short-range forecasts, especially for middle-upper tropospheric moisture, in situation awareness and nowcasting.

1. Introduction

The Advanced Baseline Imager (ABI; Schmit et al., 2005, 2017) onboard the new generation Geostationary Operational Environmental Satellite (GOES)-16 satellite, the first of GOES-R series and launched on 19 November 2016, has fine temporal (30 s to 10 min) and spatial resolutions (0.5–2 km), and 16 spectral bands. GOES-16 started a new era for the U.S. geostationary satellite observing system. However, due to the lack of an infrared (IR) sounder on the spacecraft, the ABI is used to continue the legacy atmospheric profile (LAP) products (Schmit et al., 2008) that the previous GOES Sounder (Menzel & Purdom, 1994) provided for nowcasting and weather forecasting (Menzel et al., 1998). Those LAP products from ABI include the legacy atmospheric vertical moisture profile (LVM), legacy atmospheric vertical temperature profile (LVT), total precipitable water (TPW), layered precipitable water (LPW), and derived atmospheric stability indices (DSI) over each 5 × 5 ABI pixels box area with clear-sky IR band radiances. DSI includes five atmospheric instability indices: lifted index (LI), convective available potential energy (CAPE), total totals index (TT), K-index (KI), and Showalter index (SI). The ABI LAP algorithms have been developed under the GOES-R series Algorithm Working Group program and have been validated with Spinning Enhanced Visible and Infrared Imager (SEVIRI) and GOES Sounder as proxy before GOES-16 was launched (Jin et al., 2008; Lee et al., 2014). To further evaluate the ABI LAP products for operational applications, validations have been conducted after ABI products are available in early 2017. The purpose of ABI LAP validation is to address the following questions: (1) Do all the ABI LAP products meet the requirements and how to validate? (2)

What is the added value from ABI LAP products over the NWP model short-range forecasts that are widely used by the forecasters? (3) What is the most important information that ABI LAP products can provide for nowcasting applications? In order to address those questions, methodologies and approaches have been developed at the Cooperative Institute for Meteorological Satellite Studies of the University of Wisconsin-Madison, with a series of reference data sets including radiosonde observation (RAOB) at conventional RAOB sites, Global Positioning System (GPS) from SuomiNet, and Advanced Microwave Scanning Radiometer 2 (AMSR2) TPW measurements, as well as global operational analysis from the National Oceanic and Atmospheric Administration (NOAA) and European Centre for Medium-Range Weather Forecasts (ECMWF) models. A validation webpage is also developed in near real time (http://sounding-val.ssec.wisc.edu/) for monitoring the quality of ABI LAP products.

The GOES-R ABI LAP products are retrieved using one-dimensional variational (1DVAR) algorithm based on the ABI IR band measurements with NWP (NOAA Global Forecast System, GFS) short-range forecasts as first guess. The GFS is preferred over other NOAA regional NWP models because of its global coverage. The LAP products are generated every 10 min over the ABI Full Disk (FD), every 5 min over the Continental United States (CONUS) region, and every 1 min over the mesoscale (MESO) regions. A full description and format of the LAP products can be found in the Product Definition and User's Guide document (http://www.goes-r.gov/products/docs/PUG-L2+-vol5.pdf). The algorithm used to derive the LAP products from GOES-16 ABI observations is described in detail in the "GOES-R Advanced Baseline Imager (ABI) Algorithm Theoretical Basis Document for Legacy Atmospheric Moisture Profile, Legacy Atmospheric Temperature Profile, Total Precipitable Water, and Derived Atmospheric Stability Indices" (https://www.goes-r.gov/products/ATBDs/baseline/Sounding_LAP_v2.0_no_color.pdf).

For over a year, it is found that the LAP product performance has been stable and meeting the requirements, when compared against reference data including SuomiNet GPS, AMSR2, RAOB, ECMWF analysis, and Global Data Assimilation System (GDAS) analysis, and AERI (Atmospheric Emitted Radiance Interferometer) boundary layer profiles from a GOES-16 field campaign. Accuracy specification (1 mm) and precision specification (3 mm) are met for TPW product; accuracy specification (1 K above boundary layer and below 400 hPa) and precision specification (2 K above boundary layer and below 400 hPa) are met for LVT; accuracy specification (18% between the surface and 300 hPa, 20% between 300 and 100 hPa) and precision specification (same as accuracy specification) are met for LVM; accuracy specification (2 °C, 1,000 J/kg, 1 °C, 2 °C, and 2 °C) and precision specification (6.5 °C, 2,500 J/kg, 4 °C, 5 °C, and 6.5 °C) are met for LI, CAPE, TT, KI, SI, respectively, except TT and KI when compared to RAOBs. The inclusion of only the atmospheric unstable cases makes the TT (>44) and KI (>26) results closer to the requirements. It should be noted that some of the requirements for the ABI LAP were relaxed, when the hyperspectral resolution IR sounder was canceled on the GOES-R series.

The ABI LVM has improved accuracy and precision over the NWP short-range forecasts with its three mid-level water vapor absorption bands centered at 6.3, 6.9, and 7.3 μm, respectively, when compared with RAOBs. Considering the fact that ABI has much better temporal and potential spatial resolutions than the previous GOES Sounder, it makes the water vapor products (TPW, LVM, and LPW) have unique value in nowcasting, weather forecasting, and NWP assimilation applications. For example, Lee et al. (2017) demonstrated that the frequent (10-min interval) FD LAP products over the East Asia and Western Pacific regions, derived from the Advanced Himawari Imager (AHI), which is similar to ABI, have the capability on depicting the detailed temporal features in the prelandfall environment of a typhoon. Hazardous Weather Testbed (HWT) experiments in the summer of 2017 and the spring of 2018 also indicate the ABI LAP products are specifically good for situational awareness and monitoring; the temporal and spatial gradients, time tendencies are the most important information that the forecasters like to use. With high temporal and spatial resolution LAP products, the low-level moisture advection and increasing instability can be well depicted and monitored in preconvection environment and during storm development. TPW, LPW, LI, and CAPE are the most useful products in situation awareness and nowcasting. For example, the LPW provides more vertical information than the TPW alone, and it is helpful to track the evolution of low-level moisture boundaries, as well as the relationship of moisture at the various layers to each other. Dry air moving over moistening air implies increasing convective instability and severe weather threat, while moist air over moist air implies more of a heavy rain threat. LPWs are also very useful for improving NWP model forecasts. Wang et al. (2018) found that assimilation of LPWs from AHI provides improvement on heavy precipitation forecasts of local severe

storms (LSS) over those from the assimilation of conventional data, and AHI IR band radiance assimilation and LPW assimilation show overall similar or comparable impact on precipitation forecasts. Recently, Lu et al. (2019) found that LPW assimilation reduces the average track error and speeds up tropical cyclone (TC) movement by better adjustment of the atmospheric circulation fields via changing the vertical structure of moisture and temperature profiles.

Section 2 provides descriptions on GOES-16 ABI observations, LAP algorithm, and products; section 3 provides validation results and analysis; section 4 overviews the application area with cases from 2017 and 2018 HWT experiments; and summary and future considerations are given in section 5.

2. GOES-16 Observations, LAP Algorithms, and Products

The first two (GOES-16 and GOES-17) of the GOES-R series (GOES-R, GOES-S, GOES-T, and GOES-U) were launched in November 2016 and March 2018, respectively. The ABI is the primary instrument onboard GOES-R series for observing Earth's weather (Schmit et al., 2005, 2017). The capability of ABI is a significant improvement over that of previous GOES imagers (Menzel & Purdom, 1994) with finer spatial and temporal resolutions (2 km for IR channels, 10 min for FD, plus 5 min for CONUS, and 1 min for two independent mesoscale regions), improved calibration, and image navigation and registration. However, the GOES-R series satellites do not and will not carry an advanced IR sounder, which was planned but later canceled due to budget constraints (Schmit et al., 2009). In order to continue the classic GOES Sounder LAP products, the ABI and NWP forecast profiles are used together to provide similar products. The GOES-R series ABI LAP algorithm has been developed (Jin et al., 2008; Li et al., 2000) for the retrieval of atmospheric temperature and moisture profiles from clear-sky radiance observations. From the temperature and moisture profiles, the associated TPW, LPW, and atmospheric stability indices such as LI, CAPE, TT, SI, and KI are also derived. The product generation needs IR brightness temperatures (BTs) from selected ABI channels along with NWP short-range forecast output. Although the advanced sounding products that were originally envisioned for GOES-R series cannot be realized with the Hyperspectral Environmental Suite withdrawn, legacy sounding products that are used by the National Weather Service and other agencies must be provided. Schmit et al. (2008) showed that adequate substitute products can be generated from ABI data in conjunction with information from short-term numerical model forecasts, although the quality would be slightly inferior to the GOES-13/GOES-14/GOES-15 Sounder performance, and significantly less capable than a high-spectral resolution sounder with respect to information content and retrieval accuracy (Menzel et al., 2018; Schmit et al., 2009).

ABI bands 8–16 (6.15 to 13.3 μm), which include four absorption bands (three water vapor bands and one CO_2), are the primary channels used in LAP retrieval. The 3.9-μm channel is excluded in the retrieval because it is difficult for radiative transfer models (RTMs) to simulate the observation accurately, especially during daytime. The surface emissivity (SE) of 8.5 μm has large variability over land, especially over desert, and thus, this channel is excluded in the regression retrieval. In the 1DVAR-based physical retrieval, this channel is also excluded for land, but it is included for ocean. The ozone absorption 9.7-μm channel is used only in regression to generate ozone profile and is excluded in the physical retrieval. The retrieval is performed on Field-of-Regard (FOR, default is a 5×5 pixel box area, about 10 km $\times$ 10 km but adjustable) basis, only if (a) the FOR is clear enough and (b) the satellite zenith angle is below the configurable maximum zenith threshold (67°). In order to determine a FOR is clear enough, there has to be 10 or more clear pixels within the FOR box area. In that case, the mean radiances of the clear pixels are assigned as the observation for this FOR. Therefore, the retrieval is more for clear portion of the FOR than the FOR itself. The advantage of this is increased retrieval spatial coverage. When both conditions are met, the LAP TPW, LPW, LI, CAPE, SI, KI, and TT parameters are calculated from retrieved profiles for this FOR. The algorithms have three steps:

Step 1:   The general least squares regression for first guess

The LAP algorithm uses the general least squares regression to generate the first guess with ABI IR band radiances and forecast profile as predictors. The SeeBor database (Seemann et al., 2003, 2008) is used to generate the regression coefficients. The SeeBor database comprises global temperature, humidity, and ozone profiles from TIGR3, NOAA88, and ECMWF, supplemented by profiles from desert radiosondes and ozone sondes. The total number of training set profiles is 15,704. For each profile, some surface parameters critical

for RTM calculation, such as surface skin temperature and IR SE at ABI IR bands are also accompanied. Other surface parameters such as surface pressure and surface type are also provided. The predictands include temperature/moisture/ozone profiles as well as surface skin temperature and SE. The predictors include ABI IR spectral band BTs, surface pressure, latitude, month, and land/ocean flag. Since ABI only has a few sounding spectral bands, the temperature/moisture profiles from NWP forecast model are used as additional predictors. Here we use temperature forecast between 100 and 1050 hPa and mixing ratio forecast between 300 and 1,050 hPa from GFS 6- to 12-hr forecast as additional predictors. For any predictand Z (e.g., temperature or water vapor/ozone mixing ratio at a given pressure level), the regression equation is written in the following form:

$$Z = A_0 + \sum_{j=1}^{N} B_j T_{bj} + \sum_{j=1}^{N} C_j T_{bj}^2 / 250 + \sum_{l=1}^{n} b_{tl} T_l + \sum_{l=1}^{m} b_{wl} \log(w_l) + D_1 p_s$$
$$+ D_2(\text{Lat}) + D_3(\text{mon}) + D_4(\text{Pland}) \tag{1}$$

where T_{bj} is the channel j BT; T_l and w_l are forecast temperature and water vapor mixing ratio at level l, respectively; p_s is the surface pressure; Lat is the latitude between ± 70; mon is the month between 1 and 12; Pland is the land/ocean flag (1.0 for land and 0.0 for ocean). A, B, b, C, and D_1 to D_4 are regression coefficients; N, n, and m are the number of ABI IR spectral bands, profile temperatures, and profile mixing ratios used as predictors, respectively. The mixing ratio in both predictors and predictands is in the form of logarithm because of better linear relationship to satellite-based IR radiances.

The regression problem can be simplified by assuming a linear relationship between the atmospheric state vector **X** as predictants and the measurements as well as additional predictors **Y** using $\mathbf{X} = \mathbf{C}\mathbf{Y^T}$, where **C** is the matrix of regression coefficients. The superscript **T** refers to transposition. According to the method of general least squares, where one needs to minimize the sum of the squared deviations from the data, and the solution is $\mathbf{C} = (\mathbf{Y^T \Omega^{-1} X})^{-1} \mathbf{X^T \Omega^{-1} Y}$, where Ω is the error covariance matrix of predictors. With SeeBor database (Borbas et al., 2005) as training, the regression coefficients can be derived.

The regression coefficients are applied to ABI radiance observations to generate atmospheric profiles as the first guess for physical retrieval iterations. Since the forecast profile is used together with ABI IR BTs as predictors, the regression should be no worse than the forecast.

Step 2: 1DVAR based physical retrieval

The variational retrieval is performed by adjusting the atmospheric profile state, $\boldsymbol{X}$, from the background, $\boldsymbol{X^b}$, to minimize a cost function, $\boldsymbol{J(X)}$ (Li et al., 2000, 2008; Li & Huang, 1999; Ma et al., 1999; Rodgers, 1976, 1990). The regularization parameter (also called smoothing factor) is introduced for convergence and solution stability. The cost function (Eyre et al., 1993; Li et al., 2000) is defined by

$$J(X) = [Y^m - F(X)]^T E^{-1} [Y^m - F(X)] + [X - X^b]^T \gamma B^{-1} [X - X^b] \tag{2}$$

where **Y** is a vector of ABI IR BTs (10 IR channels for ABI), $\boldsymbol{X}$ is state vector containing temperature profile $T(p)$ and moisture profile $q(p)$ on L vertical pressure levels plus the surface skin temperature, $\boldsymbol{F}$ is fast RTM (operator) for radiances, γ is the regularization parameter, $\boldsymbol{B}$ and $\boldsymbol{E}$ are the error covariance matrices of background, $\boldsymbol{X^b}$, and the observation vector (channel radiances), $\boldsymbol{Y^m}$, respectively, and superscripts $\boldsymbol{T}$ and $\boldsymbol{-1}$ are the matrix transpose and inverse, respectively. That is,

$$\boldsymbol{Y} = (y_1, y_2, ..., y_N) = (Tb_1, Tb_2, ..., Tb_N)$$
$$\boldsymbol{X} = (x_1, x_2, ..., x_{2L+1}) = (T_1, T_2, ..., T_L, \ln q_1, \ln q_2, ..., \ln q_L, T_s)$$
$$\boldsymbol{F} = (f_1, f_2, ..., f_N)$$

By using the Quasi-Newtonian (ignoring the Hessian matrix) iteration (Ma et al., 1999)

$$X_{n+1} = X_n + J''(X_n)^{-1} \cdot J'(X_n) \tag{3}$$

which states that the $(n + 1)$th iteration equals to the nth iteration plus the first order derivative of cost function divided by second-order derivative of cost function. Therefore, the following quasi-nonlinear iterative form is obtained (Li et al., 2000).

$$\delta \boldsymbol{X_{n+1}} = \left(\boldsymbol{F_n^{'T}} \cdot \boldsymbol{E^{-1}} \cdot \boldsymbol{F_n^{'}} + \gamma \boldsymbol{B^{-1}} \right)^{-1} \cdot \boldsymbol{F_n^{'T}} \cdot \boldsymbol{E^{-1}} \cdot \left(\delta \boldsymbol{Y_n} + \boldsymbol{F_n^{'}} \cdot \delta \boldsymbol{X_n} \right) \tag{4}$$

where $\delta \mathbf{X_n} = \mathbf{X_n} - \mathbf{X^b}$ and $\mathbf{X_0}$ is the first guess from regression; $\delta \mathbf{Y_n} = \mathbf{Y^m} - \mathbf{F(X_n)}$ is the difference between the measurement and the forward model calculation. $\boldsymbol{F^{'}}$ is the tangent linear operative (Jacobian) of forward model $\boldsymbol{F}$. The regularization parameter is adjusted in each iteration, according to the discrepancy principal (Li et al., 2000; Li & Huang, 1999). The reason to introduce the regularization parameter is to balance the contributions from background and satellite observations in the solution. The regression-derived profiles are used as both background and first guess in the iteration procedures. Since there are correlations among atmospheric variables, only a limited number of variables are needed to explain the vertical structure variation of an atmospheric profile (Smith & Woolf, 1976). This can be realized through eigenvectors:

$$X - X^b = \Phi A \tag{5}$$

where

$$\Phi = \begin{bmatrix} \Phi_{\mathrm{T}} & 0 & 0 \\ 0 & \Phi_{\mathrm{q}} & 0 \\ 0 & 0 & \Phi_{\mathrm{T_s}} \end{bmatrix}$$

where $\boldsymbol{\Phi}$ is the empirical orthogonal function (EOF) matrix, $\boldsymbol{\Phi_T}$ is selected EOFs of the temperature profile, $\boldsymbol{\Phi_q}$ is selected EOFs of the water vapor mixing ratio profiles, $\boldsymbol{\Phi_{T_s}} = \mathbf{1}$, and the vector $\boldsymbol{A}$ is the coefficient for EOFs. The EOFs are also derived from the training profiles used to train the regression coefficients. Since there are only one CO_2 channel and three water vapor channels from ABI used in the LAP processing, one temperature EOF and three water vapor mixing ratio EOFs are used. Define $\boldsymbol{\widetilde{F}^{'}} = \boldsymbol{F^{'}} \cdot \boldsymbol{\Phi}$, equation (5) (Li et al., 2000) becomes

$$\mathrm{A_{n+1}} = \left(\widetilde{F}_n^T \cdot \mathrm{E}^{-1} \cdot \widetilde{F}_n^{'} + \gamma \widetilde{B}^{-1} \right)^{-1} \cdot \widetilde{F}_n^T \cdot \mathrm{E}^{-1} \cdot \left(\delta Y_n + \widetilde{F}_n^{'} \cdot \mathrm{A_n} \right) \tag{6}$$

where $\widetilde{B}^{-1} = \Phi^T B^{-1} \Phi$, $\mathrm{A_0} = 0$. The iteration stops when the Tb residual is approaching observation noise.

$$\|\boldsymbol{F}(\boldsymbol{A}(\gamma)) - \boldsymbol{Y^m}\|^2 = \sigma^2 \tag{7}$$

where σ is the observation error of ABI. With the final EOF coefficients $\mathbf{A_{n+1}}$, the profiles can be obtained using equation (5). Since the retrieval is performed on one single profile, it is also called 1DVAR physical retrieval method.

Step 3:   The derived products

After the physical retrieval, the derived products are calculated from the atmospheric profiles of temperature and moisture. Sometimes, forecasters prefer those derived products than the profiles because they are more indicative of weather and better match the information content of the observations. The remaining of this section describes how these derived products are calculated.

TPW (mm) is the amount of liquid water if all the atmospheric water vapor in the column was condensed. The following equation is used to derive TPW:

$$\mathrm{TPW} = \frac{10}{\rho_w g} \sum_{k=1}^n 0.5 \cdot (q(k+1) + q(k)) \cdot \left(p_k - p_{k+1} \right) \tag{8}$$

where ρ_w is the water density; g is the standard gravitational acceleration; $q(k)$ is the mixing ratio of water vapor profile at the kth level; $p_{k=1}$ is the surface air pressure in hectopascals; $p_{k=n}$ is 300-hPa pressure level. Since the water vapor content is very rare above 300 hPa, only water vapor content between surface and 300 hPa is accumulated to derive TPW.

LI (°C) is the temperature difference between a lifted parcel and the surrounding air at 500 hPa (Galway, 1956; Petty, 2008). The parcel is lifted dry adiabatically from the mean lowest 100-hPa layer (i.e., the pressure between surface level and the level 100 hPa above the surface) to the condensation level, and then wet

adiabatically to 500 hPa. LI provides estimations of the atmospheric stability. The LI indicates the atmospheric thermodynamic instability according to its value: 0 °C < LI for stable, −3 °C < LI < 0 °C for marginally unstable, −6 °C < LI < −3 °C for moderately unstable, −9 °C < LI < −6 °C, very unstable, and LI < −9 °C for extreme unstable. It is important to point out that LI is not the only ingredient for severe storms. It has to be used in conjunction with other measurements in order to alert the forecasters about the possibility of the occurrence of mesoscale events.

CAPE (J/kg) measures the cumulative buoyancy of a parcel as it rises. Its definition (Petty, 2008) is

$$\text{CAPE} = g\sum_{k=1}^{n} \frac{0.5\cdot(T_{\text{va}}(k)-T_{\text{va}}(k-1))-0.5\cdot(T_{\text{ve}}(k)-T_{\text{ve}}(k-1))}{0.5\cdot(T_{\text{ve}}(k)-T_{\text{ve}}(k-1))+273.16}\cdot(z(k)-z(k-1)) \tag{9}$$

where Z is geopotential height, $Z_{k=1}$ is the geopotential height of free convection, $Z_{k=n}$ is the geopotential height of equilibrium level, T_{ve} and T_{va} are wet-bulb potential temperature for the environment and the air parcel, respectively; g is the standard gravitational acceleration in meters per square second. CAPE values larger than 1,000 J/kg represent moderate amounts of atmospheric potential energy. Values exceeding 3,000 J/kg are indicative of very large amounts of potential energy and are often associated with strong/severe weather. It should be noted that there are different methodologies for CAPE calculation and results should be interpreted accordingly when it is used.

TT (°C) is indicative of severe weather potential, and it is defined as (Petty, 2008)

$$\text{TT} = (T850-T500) + (T_{\text{d}}850-T500) \tag{10}$$

where T and T_{d} are air and dew point temperature in degrees Celsius, respectively. For example, $T500$ represents atmospheric temperature at 500 hPa. Generally, TT values below 40–45 °C are indicators of weak or no thunderstorm activity, while values exceeding 55 °C in the eastern and central United States or 65 °C in the western United States are indicators of considerable severe weather.

SI (°C) is a parcel-based index, calculated in the same manner as the LI, but assuming that the parcel is lifted from the 850-hPa level, instead of the lowest 100-hPa level above surface. That is, the 850-hPa parcel is lifted to its condensation level and moist adiabatically to 500 hPa. The difference between the parcel and environment at 500 hPa is the SI (Petty, 2008). An SI value smaller than −3 °C indicates the possible conditions for a severe weather.

KI (°C) is a simple index using data from discrete pressure levels instead of a lifted parcel. It is based on vertical temperature changes, moisture content of the lower atmosphere, and the vertical extent of the moist layer. The higher the KI the more conducive the atmosphere is to convection. The formula (Petty, 2008) for KI is

$$\text{KI} = (T850 + T_{\text{d}}850)-(T700-T_{\text{d}}700)-T500 \tag{11}$$

Severe weathers are very likely to occur if the value of KI exceeds 30 °C.

3. Validation

The GOES-R ABI LAP algorithm has been extensively validated both before and after the GOES-16 launch. Before the launch of GOES-16, the LAP algorithm was applied to other satellite measurements, such as SEVIRI (Jin et al., 2008; Xie et al., 2013), the legacy GOES Sounders (Lee et al., 2014), and AHI (Bessho et al., 2016; Lee et al., 2017) for extensively testing of the sounding products, including temperature/moisture profiles and derived products, such as TPW, LPW, LI, CAPE, SI, KI, and TT, against numerous independent sources of measurements. These measurements included conventional RAOBs, AMSR for Earth Observing System TPW over ocean, ECMWF analysis, the RAOB and microwave radiometer measured TPW at the ARM CART site, and the GPS TPW (Birkenheuer & Gutman, 2005). These prelaunch validations ensure the quality of the ABI LAP sounding and derived products for future operational use.
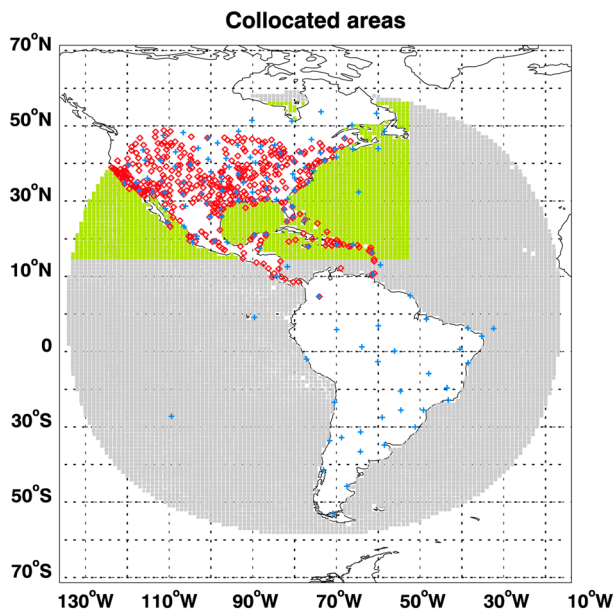
Figure 1. Collocated regions of Advanced Microwave Scanning Radiometer 2 for the Geostationary Operational Environmental Satellite 16 Full Disk (gray) and Continental United States (green), SuomiNet Global Positioning System (red diamond), and radiosonde observation (blue cross).

After the launch, the ABI LAP algorithm has gone through a series of validation stages, including Beta and Provisional Maturity. The Beta Maturity is an early preview of the product, which is very minimally validated over a short period of time (about 1 month for LAP). Products after Beta maturity are not necessarily optimal but contain no major defects and thus are not ready for operational use. During the provisional maturity stage (about 9 months for LAP for GOES-16), products are validated through analysis of a small number of independent measurements obtained from selected locations, time periods, and associated ground truth/field program efforts. This study shows the comprehensive validation results from an extended period of time (May 2017 to August 2018, provisional stage plus additional 5 months), in all three domains (FD, CONUS, and MESO), using different sources of reference measurements, including conventional RAOB, SuomiNet GPS TPW, AMSR2 TPW over ocean, ECMWF analysis, GDAS analysis, and field campaign of AERI measurements. These validation results show that the GOES-16 LAP and derived products meet the requirements, are ready for operational use, and provide added information over the GFS first guess. The ABI LAP products are available in NetCDF via NOAA's Comprehensive Large Array-data Stewardship System.

3.1. Validation References
3.1.1. Conventional RAOB

Conventional RAOB from stations located within the GOES-16 observation coverage—149 stations within the FD and 105 stations within the CONUS area—are used for the validation of ABI LAP and derived products. The locations of RAOB sites used in the study are shown in Figure 1 in blue crosses. Conventional RAOB database is a merge of Global Telecommunications System data available through NOAA National Climatic Data Center's Integrated Global Radiosonde Archive project with the observations collected at the Earth Systems Research Laboratory/Global Systems Division. Therefore, the accuracy, precision, and completeness of data can vary over time and among stations. However, a comprehensive set of quality control has been applied to remove gross errors (Durre et al., 2006). RAOB has been widely used in satellite sounding product validation (Jin et al., 2008; Lee et al., 2014; Li et al., 2008, 2009; Ma et al., 1999; Weisz et al., 2007).

For the validation of ABI LAP products, the 12-hr interval RAOB data were collected from May 2017 to August 2018 and collocation of the RAOB and GOES-16 were done within a 0.2° radius distance. TPW, LPW, and five stability indices are directly calculated from the RAOB temperature/moisture profiles for the comparisons.

3.1.2. AMSR2

For the evaluation of ABI TPW over the ocean, measurements from AMSR2 onboard the Global Change Observation Mission-Water 1 satellite of Japan are used. AMSR2 TPW are statistically derived from the BTs measured from four AMSR2 channels and by applying a wind direction correction (Chang et al., 2015), and the known accuracy of AMSR2 TPW is 1.5 and 2.6 mm RMS with respect to GPS and RAOB, respectively (https://suzaku.eorc.jaxa.jp/GCOM_W/materials/product/AMSR2_L2_2.pdf). Around 7.8 million AMSR2 data within ABI FD coverage (gray area in Figure 1; 0.8 million for the CONUS area; green area in Figure 1) are used to evaluate the ABI TPW between May 2017 and August 2018. The collocation criteria between ABI and AMSR2 are set by a time difference of less than 30 min and a horizontal distance of less than 0.2°.

3.1.3. GPS

Ground-based GPS observations have been widely used due to the all-weather capabilities, high temporal resolution, and high accuracy of better than 2 mm in TPW: about 1–1.5 mm RMS with respect to water vapor radiometers and radiosondes (Rocken et al., 1997). To evaluate ABI TPW product, TPW estimated from SuomiNet GPS (Ware et al., 2000) network is utilized. TPW data from around 431 GPS sites located in the Northern Hemisphere (red diamonds in Figure 1) are collected. The GPS data are available every 30 min, and for the comparison, the ABI data with time difference less than 30 min and within 0.2° radius are

averaged. Additionally, the GPS data have been checked for quality control since it has been found that some GPS stations consistently provide data with systematic bias or extremely large TPW values, which were excluded from the evaluation.

3.1.4. ECMWF Analysis

The ECMWF analysis data are used to evaluate the ABI baseline products over land and sea. The analysis are provided in GRIB format every 6 hr (00/06/12/18Z) at 0.25° spatial resolution. For the comparisons, ABI pixels are spatially collocated with the ECMWF within 0.125° radius distance, and the ECMWF temperature/moisture profiles at 91 pressure levels are interpolated to the 101 legacy pressure levels (from 1,100 to 0.005 hPa) that has been used for GOES sounding products (Li et al., 2008, 2009). ECMWF TPW, LPW, and five stability indices are calculated from the interpolated temperature/moisture profiles for the comparisons.

3.1.5. GFS (Background)

To show improvements of ABI products over the background, that is, GFS model forecasts produced by the National Centers for Environmental Prediction, this study compares the GFS forecasts with the ABI LAP and derived products using the reference data such as conventional RAOB, ECMWF analysis, and AMSR2 TPW measurements (will be introduced in the next section). The GFS forecast are provided in GRIB format at 0.5° × 0.5° horizontal resolution and for 26 levels from 1000 to 100 hPa. The 6–12 hr GFS forecast are spatially and temporally interpolated to ABI at the time of retrieval. Spatially, they are interpolated to the 10-km × 10-km ABI pixels and temporally, two different GFS forecast times are linearly interpolated to the satellite time with time difference (Li et al., 2012).

The spatial and temporal resolution of each reference data set and the collocation criteria with GOES-16 are summarized in Table 1. The collocations between the reference and GOES-16 LAP products over FD are limited to the area with satellite zenith angle less than 67°.

3.2. Validation on ABI LAPs

The ABI LAP products are generated in clear sky at a 10-km × 10-km (or 5 × 5 ABI pixels) spatial resolution. The provisional test for the ABI LAP products used reference data such as RAOB, ECMWF analysis, GPS, AMSR2, and AERI from April 2017 to January 2018 and the validation results revealed that the product performance meets the requirements. In this study, validation has been performed over an extended period, that is, from May 2017 to August 2018, to show that the performance of ABI products is stable. In addition, the performance statistics of ABI moisture products is compared with that of GFS forecast to show that ABI improves upon the model background.

For the validation of GOES-16 LVT and LVM profiles, conventional RAOB and ECMWF analysis data were utilized. All available conventional RAOB data from 00Z and 12Z between May 2017 and August 2018 are used for the validation of the ABI retrievals over the GOES-16 FD and CONUS area, and the ABI data within 0.2° distance from each RAOB station are averaged for the comparisons. The 6-hourly ECMWF analysis data are also used for the evaluation of ABI LVT and LVM profiles and the analysis data produced at 00Z, 06Z, 12Z, and 18Z from the first day of each month between May 2017 and August 2018 are selected and paired with the ABI pixels within 0.125° (half of the ECMWF spatial resolution) distance.

The mean bias and the standard deviation (STD) between the ABI retrievals and the reference data over CONUS area are shown in Figure 2. The vertical distributions of the bias (solid lines) and STD (dotted lines) for the two different references, that is, RAOB (blue) and ECMWF (black), reveal the different characteristics of observation and model. Overall, however, both LVT (Figure 2a) and LVM (Figure 2b), are in good agreement with the reference. From the boundary layer up to 200 hPa, the mean bias of LVT with respect to RAOB and ECMWF are 0.01 K and −0.06 K, respectively, and the STD are 0.94 and 0.75 K, meeting the specifications required for GOES-16 LVT product.

The LVM (Figure 2b), in terms of relative humidity, also shows good agreement with the two references with mean bias of 4.98% and −0.91% and STD of 13.1% and 14.5% compared with the RAOB and ECMWF, respectively, between the surface and 200 hPa. The results are very similar to those of GOES-13 sounder by Lee et al. (2014), who applied the GOES-16 ABI LAP retrieval algorithm to GOES-13 sounder data and evaluated the results with conventional RAOB and other reference data. However, the figure shows that both bias and STD increase in the upper atmosphere, displaying wet bias with respect to RAOB and dry bias in comparison

Table 1
Temporal and Spatial Resolutions of the Five Reference Data Sets Used in the Study and the Collocation Criteria

Reference	Temporal resolution	Spatial resolution	Collocation criteria
Conventional RAOB	12 hr	149 stations	0.2°, ±30 min
AMSR2	two to three times per day	15 km	0.2°, ±30 min,
GPS	30 min	411 stations	0.2°, ±30 min
ECMWF analysis	6 hr	0.25°	0.125°
GFS forecast	1 hr	0.5°	10 km, linear interpolation

Note. RAOB = radiosonde observation; AMSR2 = Advanced Microwave Scanning Radiometer 2; GPS = Global Positioning System; ECMWF = European Centre for Medium-Range Weather Forecasts; GFS = Global Forecast System.

with ECMWF. The wet bias shown in the LAP moisture in comparison with RAOB is partly attributed to the dry bias of RAOB in the upper troposphere since the radiosondes launched over the US during 2017 and 2018 were dominated by LMS-6 and RS92 and those sensors tend to have dry bias in the upper troposphere (Turner et al., 2003). In addition, it is known that NCEP and ECMWF model moisture profiles tend to be wet biased and the dry bias of LAP moisture with respect to ECMWF between 300 and 200 hPa could reflect that nature. To get more reliable validation results, future study will include bias-corrected reference such as radiosonde data produced by the Global Climate Observing System Reference Upper-Air Network (Sun et al., 2017) software, when they become regularly available.

The AERI is a ground-based passive IR spectrometer, providing hyperspectral downward radiances emitted by the atmosphere. The atmospheric sounding retrievals from AERI radiances (Turner & Lohnert, 2014) have been shown with good quality, especially in the lower atmosphere (i.e., below 2 km). The evaluation of ABI profiles using one-month (22 May to 22 June 2017) of AERI sounding products from a GOES-16 field campaign has also revealed a mean bias of −0.9 K and an STD of 1.2 K for the boundary layer temperature profiles (up to 700 hPa) and 6.7% mean bias and 11. 8% STD for the boundary layer humidity profiles (not shown).
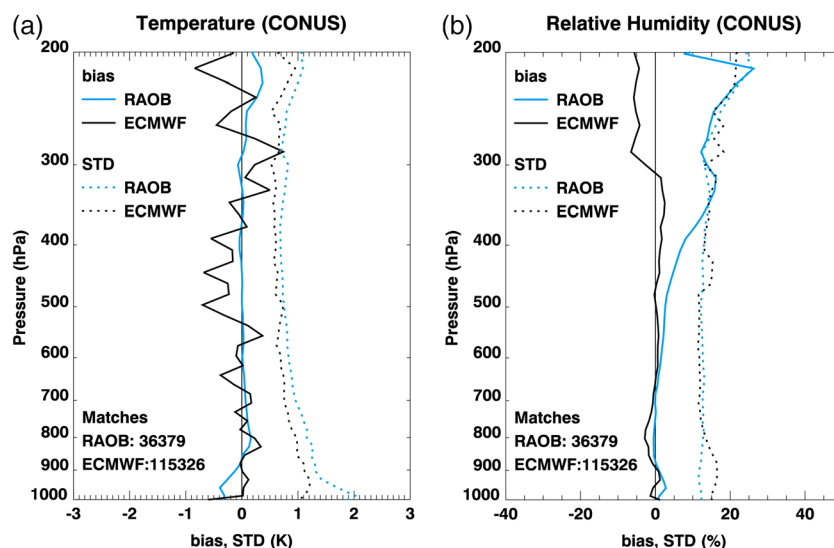

Figure 2. Comparisons of Geostationary Operational Environmental Satellite 16 Advanced Baseline Imager (a) legacy atmospheric vertical temperature profile and (b) legacy atmospheric vertical moisture profile profiles with RAOB (blue lines) and ECMWF analysis (black lines) over CONUS. The solid lines are mean bias averaged for the space and time and the dotted lines are STD of the differences. RAOB = radiosonde observation; ECMWF = European Centre for Medium-Range Weather Forecasts; STD = standard deviation; CONUS = Continental United States.
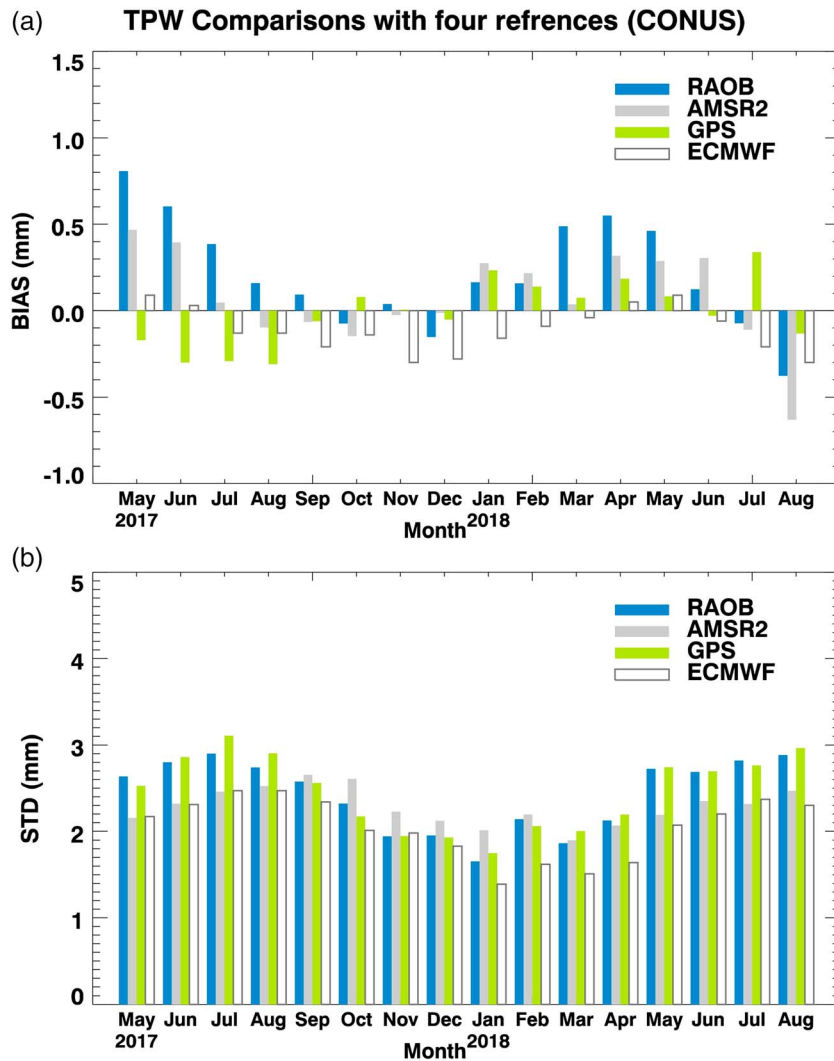
Figure 3. Intercomparisons of monthly (a) mean bias and (b) STD between Advanced Baseline Imager TPW and RAOB (blue), AMSR2 (gray), SuomiNet GPS (green), and ECMWF analysis (white) over CONUS from May 2017 to August 2018. RAOB = radiosonde observation; AMSR2 = Advanced Microwave Scanning Radiometer 2; GPS = Global Positioning System; ECMWF = European Centre for Medium-Range Weather Forecasts; STD = standard deviation; CONUS = Continental United States; TPW = total precipitable water.

Table 2
Bias, STD, and RMSD Between the Reference (RAOB, AMSR2, GPS, and ECMWF) and GOES-16 ABI TPW for the FD, CONUS, MESO1, and MESO2 Domains

	FD			CONUS			MESO1			MESO2		
Reference	Bias	STD	RMSD	Bias	STD	RMSD	Bias	STD	RMSD	Bias	STD	RMSD
RAOB	0.16	2.60	2.62	0.21	2.46	2.48	0.81	2.13	2.36	0.92	2.27	2.54
AMSR2	0.14	2.11	2.11	−0.08	2.31	2.33	0.50	2.49	2.68	0.81	2.07	2.29
GPS	0.00	2.58	2.58	−0.05	2.45	2.45	0.36	2.35	2.41	0.46	2.05	2.13
ECMWF	−0.24	2.05	2.07	−0.10	1.95	1.95	−0.03	2.16	2.17	−0.13	2.17	2.20

Note. Statistics were averaged between May 2017 and August 2018. RAOB = radiosonde observation; AMSR2 = Advanced Microwave Scanning Radiometer 2; GPS = Global Positioning System; ECMWF = European Centre for Medium-Range Weather Forecasts; STD = standard deviation; RMSD = root-mean-square deviation; GOES = Geostationary Operational Environmental Satellite; ABI = Advanced Baseline Imager; TPW = total precipitable water; FD = Full Disk; CONUS = Continental United States; MESO = mesoscale.
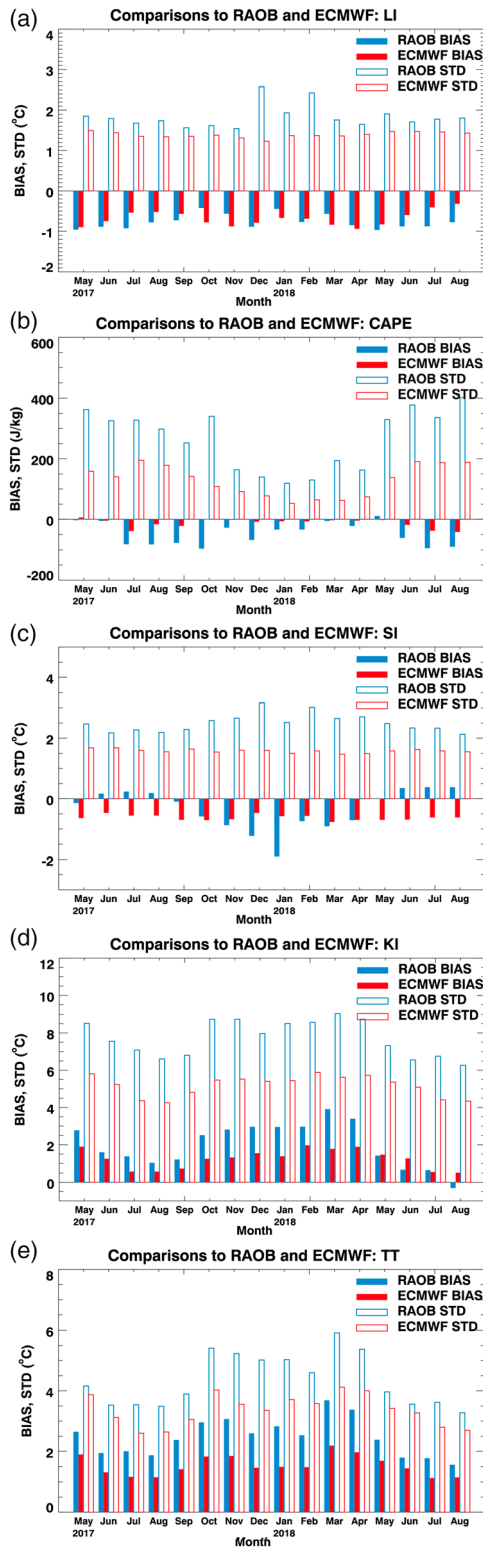
Figure 4. Time series of monthly mean bias and STD for Advanced Baseline Imager-derived (a) LI, (b) CAPE, (c) SI, (d) KI, and (e) TT with respect to RAOB (blue) and ECMWF (red). RAOB = radiosonde observation; ECMWF = European Centre for Medium-Range Weather Forecasts; STD = standard deviation; LI = lifted index; CAPE = convective available potential energy; SI = Showalter index; KI = K-index; TT = total totals index.

3.3. Validation on Derived Products
3.3.1. TPW

ABI-derived TPW and the three LPWs can be of particular importance for weather forecasting since they are indicators of possible strong flood or severe weather events. Provided with high spatial and temporal resolutions, these moisture products will add value over model forecasts, if only they are provided with good accuracy. To estimate the accuracy and performance of the ABI-derived TPW, four different types of reference data are used in this study, and those include the conventional RAOB, AMSR2, SuomiNet GPS, and ECMWF 6-hr analysis. The validation results for LPWs are presented in section 3.4.

The RAOB TPW and GPS TPW are used for the validation of ABI TPW over land, the AMSR2 TPW over the ocean, and ECMWF TPW for both land and ocean. The TPW of RAOB and ECMWF were individually calculated from their humidity profiles. The validation has been performed for clear-sky ABI TPW over the FD and CONUS domain of GOES-16 and the time period selected for the evaluation is May 2017 to August 2018.

The monthly mean bias and STD of ABI TPW were calculated individually for each of the four references and the statistics were averaged over the validation domain. Figure 3 shows the time series of monthly mean bias (Figure 3a) and STD (Figure 3b) using different references over CONUS domain during the validation period. The requirement for ABI TPW is 1 mm for accuracy and 3 mm for precision (Li et al., 2012), and as can be seen in the figure, the mean bias values of ABI TPW are well below 1 mm throughout the validation period regardless of the reference types. The time series of monthly STD displays a seasonal pattern, higher STD during the summer wet months and lower STD for the winter dry months, but they all meet the requirements except for those against GPS in July 2017. It should be noted that some of the SuomiNet GPS data have quality issues, displaying systematic bias against other references or having extremely large values over 100 up to 700 mm for the validation period. For this reason, seven GPS stations that provide data with these issues were excluded from the validation. Additionally, data from GPS stations located above 850 hPa are not used for the validation of LAP products since they may not good representatives of the area covered by ABI 5 × 5 FOR. The validation accuracy and precision for the FD and the two MESO domains (MESO1 and MESO2) all meet the specification with mean bias ranging from −0.24 to 0.92 mm and STD ranging from 1.95 to 2.60 mm as summarized in Table 2.

The statistics obtained from the provisional maturity stage using GDAS analysis (not shown) also reveals good performance of ABI TPW with mean bias of −0.6, −0.7, −0.8, and −0.6 mm for the FD, CONUS, MESO1, and MESO2 domains, respectively, and with STD of 1.5, 1.5, 1.2, and 1.2 mm for the four domains, respectively.

3.3.2. DSI

Five kinds of atmospheric instability indices, that is, LI, CAPE, SI, KI, and TT, are derived from the ABI legacy temperature and moisture profiles at 10-km spatial resolutions under clear-sky conditions. Monitoring the distributions and evolutions of these indices together with TPW can aid to investigate rapid development of convective cells
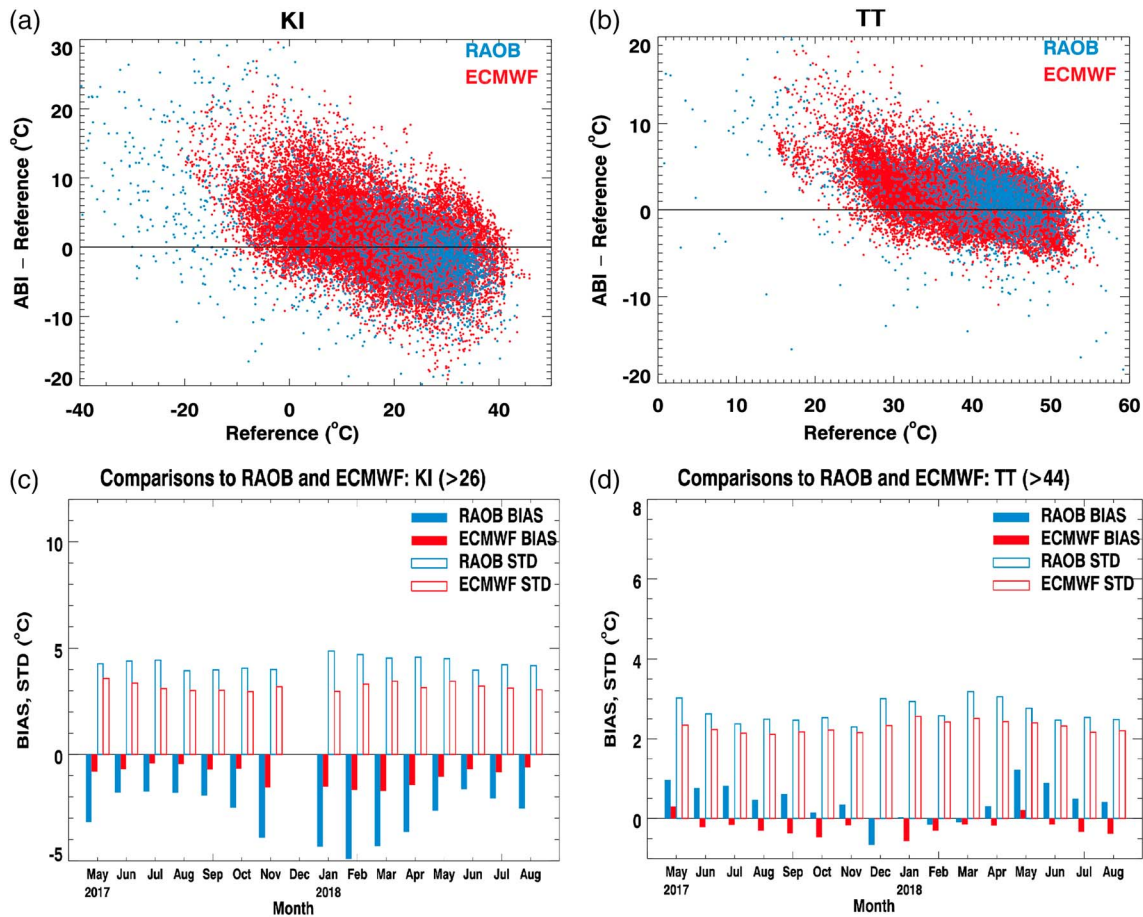
Figure 5. Difference of ABI (a) KI and (b) TT from reference (RAOB [blue dots] and ECMWF [red dots]) as a function of the magnitude of reference and time series of bias and STD of ABI (c) KI and (d) TT compared with RAOB and ECMWF under unstable atmospheric conditions (KI > 26; TT > 44). RAOB = radiosonde observation; ECMWF = European Centre for Medium-Range Weather Forecasts; STD = standard deviation; ABI = Advanced Baseline Imager; KI = K-index; TT = total totals index.

from the preconvective stage and to predict severe weather events under thermodynamically unstable atmospheric conditions. For the evaluation of ABI DSI, conventional RAOB and ECMWF analysis data are used. Figure 4 shows the times series of monthly statistics (mean bias and STD) of ABI DSI products compared with RAOB (blue) and ECMWF analysis (red) over GOES-16 CONUS area during the validation period, that is, May 2017 throughout August 2018.

The requirements for LI are 2 °C for accuracy and 6.5 °C for precision, and as can be seen in Figure 4a, the monthly mean bias of LI are less than 1 °C for the whole time period with respect to both RAOB and ECMWF. The relatively high STD values against RAOB in December 2017 and February 2018 are attributed to the data from a station located in Nassau of the Bahamas, and the STD decrease below 2 °C if the station is excluded from the evaluation. CAPE usually has large variations, ranging from 0 to 5,000 J/kg depending on season and atmospheric conditions, and hence, the requirements are quite loose; 1,000 J/kg for accuracy and 2,500 J/kg for precision. As shown in Figure 4b the ABI CAPE are in good agreement with both RAOB and ECMWF, having monthly mean bias and STD smaller than 100 and 400 J/kg, respectively. Similarly, the ABI SI (Figure 4c) also show good agreement with the two reference data, meeting the requirements (2 °C for accuracy, 6.5 °C for precision) during the whole validation period.

However, comparisons of ABI KI and TT with the references, particularly with RAOB, do not present within specification statistics (Figures 4d and 4e), failing to meet the requirements (2 °C and 1 °C for accuracy and 5 °C and 4 °C for precision, for KI and TT, respectively). A more detailed analysis of the validation results reveals that the two indices show better performance with increasing values as displayed in
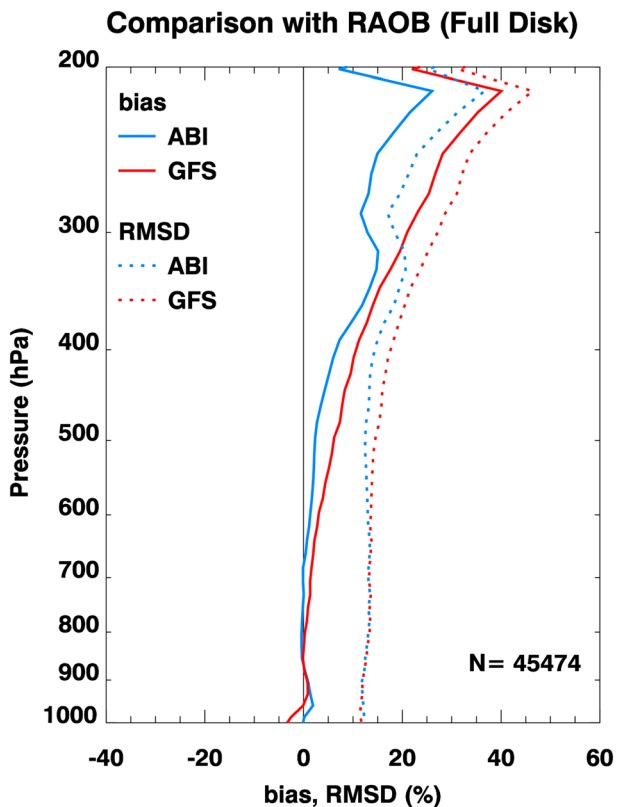
Figure 6. Mean bias and RMSD of ABI relative humidity (blue) and GFS background (red) compared with RAOB between May 2017 and August 2018. RAOB = radiosonde observation; ABI = Advanced Baseline Imager; GFS = Global Forecast System; RMSD = root-mean-square deviation.

Figures 5a and 5b. Since high values of KI and TT both indicate severe weather potential, it can be interpreted that the two indices are more reliable to use for unstable atmospheric conditions, which is the purpose of using the instability indices.

The definition of an "unstable condition," or a possible condition for a severe weather, can differ by countries or even by the states within the CONUS. For example, in the eastern and central United States, the TT values exceeding 55 indicate considerable severe weather, but in the western United States such weather conditions are expected when the TT values exceed 65 (Li et al., 2012). For this study, the unstable conditions are defined when TT values are higher than 44 (or KI values are higher than 26), and as shown in Figures 5c and 5d, the STD for both KI and TT noticeably decrease, meeting the requirements overall if validation includes only unstable cases. The accuracy (or mean bias), however, remains high for KI in particular, which will need improvements in future studies. The missing statistics in the figure is due to the small number of samples for unstable cases in December 2017, when GOES-16 was in transition eastwardly to the current position (75.2°W).

It should be noted that the difference in vertical resolutions between RAOB and LAP products can affect the computation of instability indices, hence the validation results. Unlike ECMWF instability indices, which are computed from the ECMWF profiles (91 levels) that are vertically interpolated to the legacy pressure levels (101 levels), the study directly utilizes the RAOB indices provided from the NOAA data center.

ABI TWP had also been compared with GDAS analysis during the provisional maturity stage, and the results indicate that all DSI products meet the requirements with mean bias of 0.11 °C, −43 J/kg, 0.1 °C, −0.8 °C, and −0.3 °C for LI, CAPE, SI, KI, and TT, respectively and STD of 0.8 °C, 86 J/kg, 1.0 °C, 3.3 °C, and 2.2 °C, respectively.

3.4. Added Value Over GFS Background

Comparisons have been performed between ABI products and GFS background to show added value of ABI over GFS, with RAOB as reference. Since ABI has three water vapor absorption channels with weighting function peaks at three different altitudes, improvements over GFS are expected in the moisture products of ABI such as LVM, TPW, and LPW. The potential performance of ABI moisture products was suggested by Lee et al. (2014), who applied the GOES-16 ABI LAP retrieval algorithm to the clear-sky radiance measured from the GOES-13 sounder. Their study showed that the moisture profiles retrieved from GOES-13 sounder, which also has three water vapor channels centered at 6.5, 7.0, and 7.4 μm, improved the GFS background between 700 and 300 hPa when compared with the conventional RAOB.

The comparison of the GOES-16 ABI LVM with the conventional RAOB in this study presents similar results, that is, visible improvements of ABI over GFS particularly at the mid and upper atmosphere, as displayed in Figure 6. Total 45,474 matches from May 2017 to August 2018 were compared and the ABI LVM improves the GFS relative humidity background bias and root-mean-square deviation (RMSD) by 4% and 3%, respectively, on average between the surface and 200 hPa. To further analyze where in the atmosphere improvements are more significant, the three LPWs of ABI were compared with those from GFS background.

Although not an ABI operational product, LPW products can be calculated from the ABI LVM to depict moisture content in three atmospheric layers: from the surface (or 1.0) to 0.9, 0.9 to 0.7, and 0.7 to 0.3 in sigma coordinate, or LPW1, LPW2, and LPW3, respectively (Li et al., 2012). For a reasonable comparison between different data sets, the same method used to compute the ABI LPW is applied to the computation of LPWs from RAOB and GFS forecast moisture profiles. As can be expected from the moisture profile comparisons
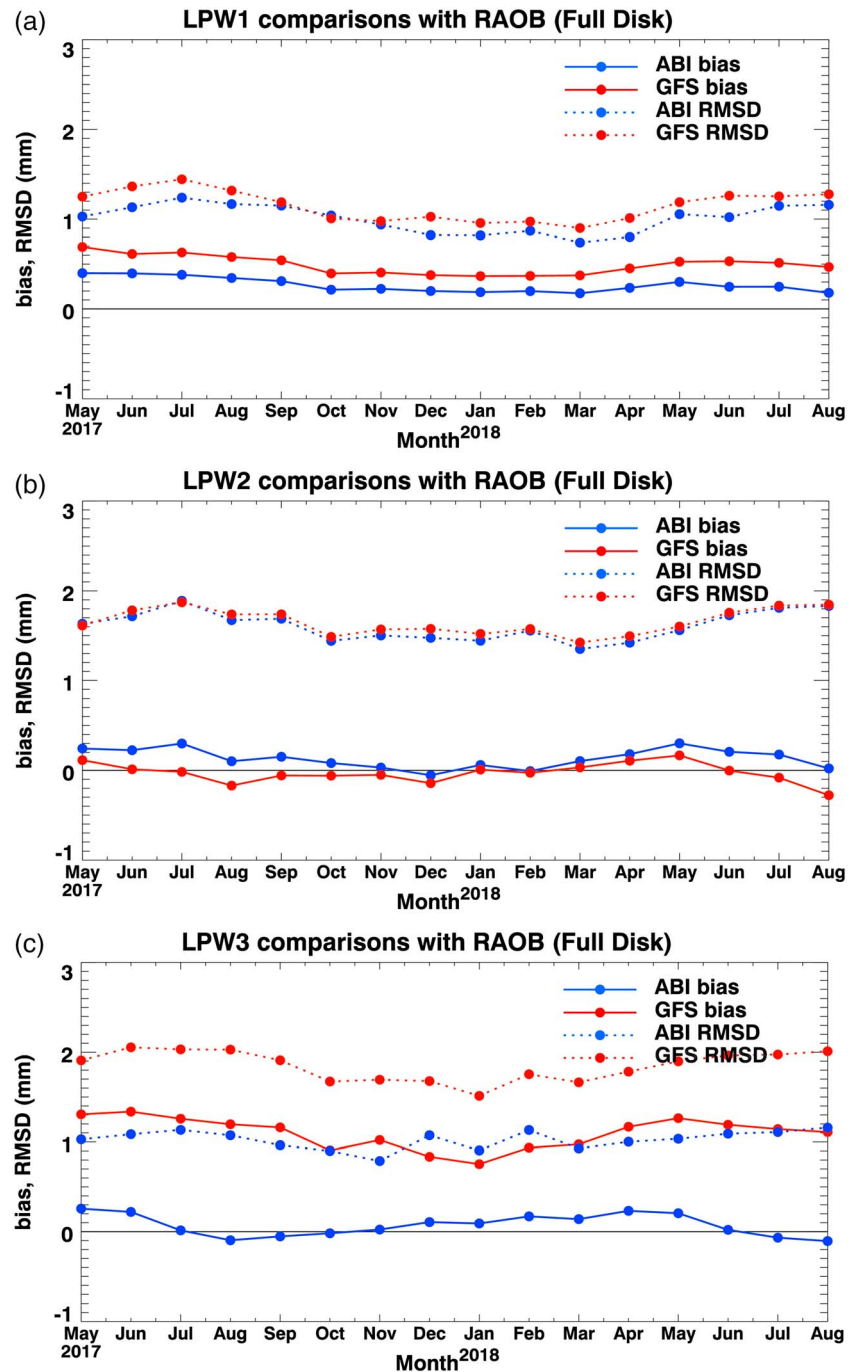
Figure 7. Time series of monthly mean statistics of ABI (blue) and GFS (red) with respect to RAOB (a) LPW1, (b) LPW2, and (c) LPW3 over Geostationary Operational Environmental Satellite 16 Full Disk from May 2017 to August 2018. ABI = Advanced Baseline Imager; GFS = Global Forecast System; RMSD = root-mean-square deviation; RAOB = radiosonde observation; LPW = layered precipitable water.

above, the most significant improvement of ABI over GFS is shown in the LPW3, the water vapor contents in the high atmospheric layer, when the conventional RAOB are used as reference (Figure 7c). In the lower atmospheric layer, ABI LPW1 also has reduced bias and RMSD from the GFS forecast (Figure 7a).

The comparison of TPW from ABI and GFS with AMSR2 observations (Figure 8) also show consistent improvements of ABI over GFS background throughout the validation period, although the magnitudes of bias and RMSD difference are not big between the two TPWs. The results suggest that over the GOES-16
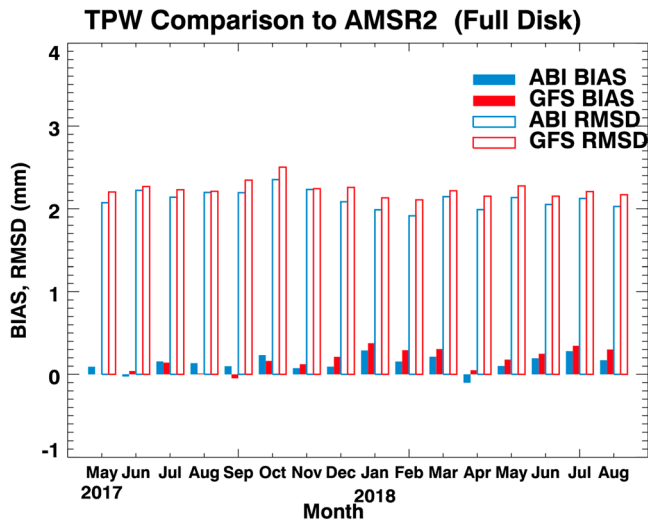
TPW Comparison to AMSR2 (Full Disk)

Figure 8. Time series of mean bias and RMSD of TPW derived from ABI (blue) and GFS forecast (red) compared with AMSR2 over Geostationary Operational Environmental Satellite 16 Full Disk between May 2017 and August 2018. ABI = Advanced Baseline Imager; GFS = Global Forecast System; RMSD = root-mean-square deviation; TPW = total precipitable water; AMSR2 = Advanced Microwave Scanning Radiometer 2.

FD ocean, both TPWs derived from ABI and GFS forecast have good performance, having mean bias smaller than 0.3 and 0.4 mm and RMSD smaller than 2.3 and 2.5 mm for ABI and GFS, respectively.

Overall, the validation results suggest that the ABI products can continue the GOES sounder legacy products with good performance. Particularly, the comparisons of ABI moisture products with the GFS background show that ABI add value over the GFS forecast, especially in the high atmospheric layer between 700 and 300 hPa.

4. Applications

4.1. Nowcasting

The GOES-16 baseline clear-sky LAP products were assessed for 2017 HWT summer experiments and forecast applications; the products were primarily utilized at the beginning of the shift each day prior to convective initiation to aid in preconvective mesoscale analysis. The PW fields were found to be helpful in assessing moisture trends and moisture return into the region of interest. For the most part, the PW fields seemed to match up well with other analysis tools which gave the forecasters confidence in using these products in their forecasts. CAPE and LI were also useful in helping forecasters understand areas with the greatest instability. These parameter values were often looked at in a relative sense, with attention on the spatial and temporal gradients since the gradients and boundaries matched up well. Forecasters found it more beneficial to take note of the trends in the updating fields as the rapid increase and moisture and instability often represented regions of future convective development. Furthermore, forecasters found that the LAP products appeared to accurately detect the location and movement of boundaries and local max/min values, which served as a focus area for convective initiation. Forecasters also mentioned that the KI, SI, and TT fields are dated and rarely used in operations anymore and could be replaced with more relevant parameters.

Although not operational, blended all-sky GOES-16 moisture and stability fields were also demonstrated in the 2018 HWT spring experiments. These products are derived via a fusion of GOES-16 radiance observations and NWP forecast data. There are three components in the all-sky products generation. The first component is the GOES-R series LAP retrieval algorithm as described above, and the LAP algorithm generates retrievals in the "clear-sky" using information from GOES-16 ABI radiances and the GFS NWP model forecasts as a first guess. The second component computes retrievals in some cloudy regions (Li et al., 2009), mainly thin/low clouds, also using information from ABI and a GFS first guess. Finally, the GFS NWP model "fills in" the areas where no retrievals are available from the previous two algorithms due to extensive sufficient cloud cover. Combining these components together provides one blended all sky. The layered PW fields proved to be beneficial in a number of cases while analyzing the preconvective environments.

There are many cases where HWT forecasters have applauded the LAP sounding products in helping them with severe storm nowcasting and forecasting, as shown online (http://goesrhwt.blogspot.com/search/label/GOES-R%20LAP). One such case was in the Des Moines, Iowa, County Warning Area (CWA) on 3 May 2018. During the early afternoon mesoscale analysis, the forecaster noticed that the two lower layers show relatively high levels of moisture over the area, while the upper level reveals a nose of dryer air advancing toward the CWA (Figure 9). The forecaster noted that this should increase convective instability throughout the afternoon and that initiation would begin on this tongue of dry mid to upper level air. As the afternoon progressed, severe thunderstorms fired along this gradient in dry air aloft and moved across the Des Moines CWA.

The main finding of the HWT Spring/Summer Experiments is that LAP products were useful for tracking gradients and min/max and trends in instability/moisture. The TPW and LPW are reasonably accurate in both values and locations. The instability indices are overall good, but CAPE seems to be underdone compared with Storm Prediction Center mesoanalysis. With the 15-min refresh rate for FD, the animation of TPW
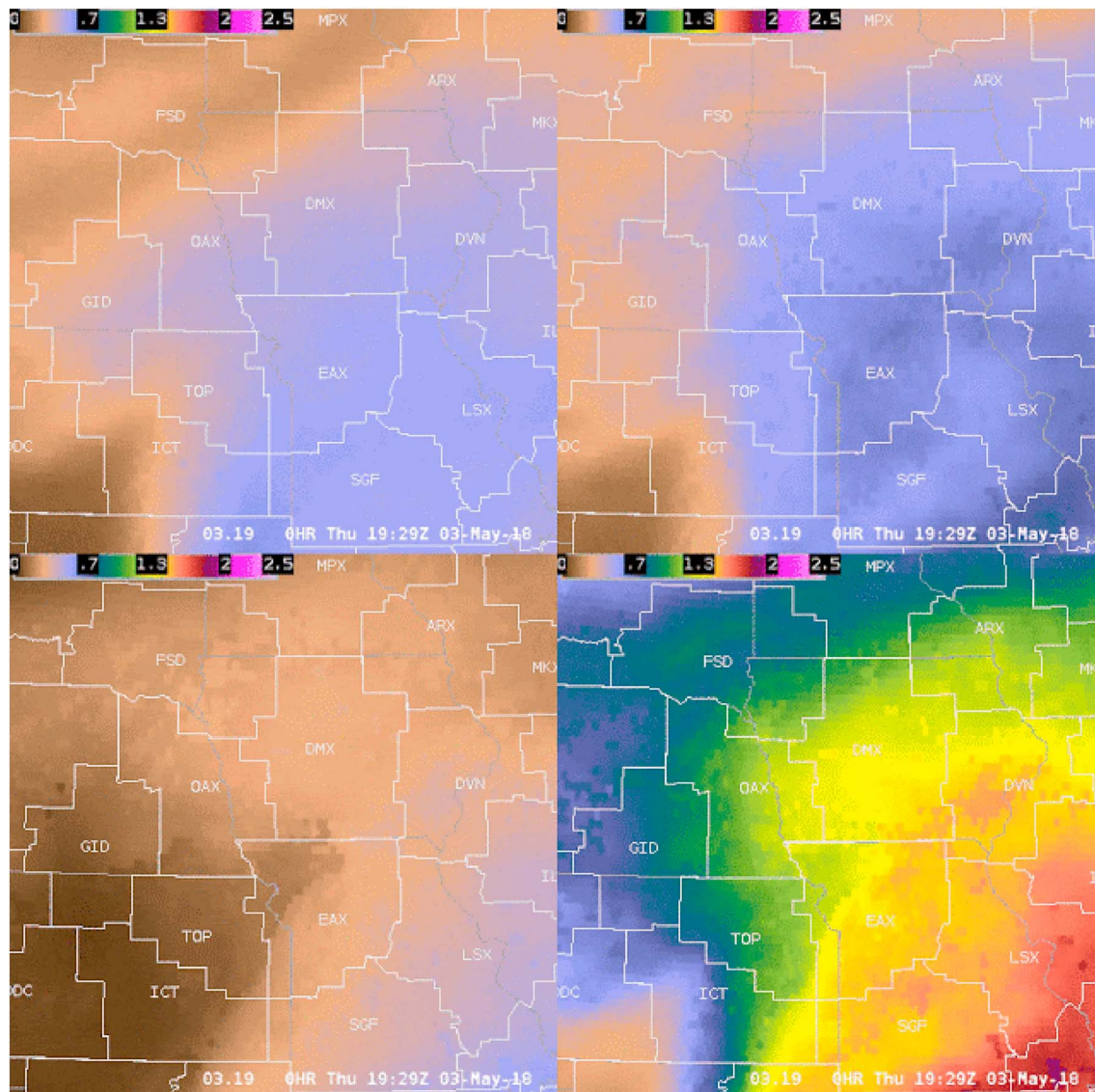
Figure 9. The 3 May 2018 1929 UTC legacy atmospheric profile layered precipitable water fields. Surface to 0.9 sigma level (upper left), 0.9–0.7 sigma level (upper right), 0.7–0.3 sigma level (lower left), and total precipitable water (lower right) across the Midwest.

and instabilities provides useful information about the development and strength of deep convection. Since April 2019, the ABI now routinely provides 10-min FD sector imagery. Together with other measurements, the LAP sounding products provide additional useful information for short-term weather forecasting and nowcasting. According to feedback from the forecasters, the TPW, LPW, and CAPE are the most important products for situation awareness and nowcasting applications. The temporal changes are specifically useful for rapid changing weather monitoring and warning. Lee et al. (2017) indicated that with the capability of frequent (10-min interval) FD observations over the East Asia and Western Pacific regions, the AHI measurements can capture the atmospheric temporal variation in the prelandfall environment for typhoon Nangka (2015), especially for those changes happened within 1 hr.

4.2. Data Assimilation in NWP Models

Information about moisture distribution and transportation in the preconvection environment is very important for nowcasting and forecasting severe weather events. Another important application of the ABI LPW product is to improve LSS forecasts through assimilating high temporal and spatial resolution moisture

information into regional and storm-scale NWP models. Wang et al. (2018) found the improvement from assimilation of LPW in storm-scale NWP model on heavy precipitation forecasts over those from the assimilation of conventional data. Comparisons between IR band radiance assimilation and LPW assimilation show overall similar or comparable impact on precipitation forecasts, but LPW assimilation provides better impact over land than that of radiance assimilation. Lu et al. (2019) also found that LPW assimilation reduces the 0- to 72hr (hour) average TC track error by better adjusting the atmospheric circulation fields, regardless which microphysical scheme and cumulus parameterization are used. They also found that LPW assimilation improves the TC intensity prediction due to accurate adjustment to the latent heat release process, the heavy precipitation forecasts are more sensitive to microphysical schemes selection, however, after LPW assimilation, the equitable threat scores from different schemes become similar and all forecast skills are increased. Those recent progress on LSS and TC forecast improvement by assimilating LPW indicates the potential operational application of LPW in NWP.

5. Summary

Due to the lack of the dedicated advanced sounder on GOES-R series, the ABI is used to generate the LAP products. With only three midlevel water vapor bands and one CO_2 band, the GFS 6 to 12-hr forecast profiles are used as background to help improve the regression retrievals. The regression retrievals are used as first guess for the physical 1DVAR retrieval iterations. The retrieved sounding products are used to generate derived products, including TPW, LI, CAPE, SI, KI, and TT. The retrieved sounding and derived products have been extensively validated using various measurements, including in situ, other satellite measurements, and NWP analysis, both before and after the GOES-16 launch. The GOES-16 ABI derived products have been shown useful to short-term severe storm forecasting and nowcasting, as demonstrated at the HWT Spring/Summer Experiments. The LPW can also provide positive impact on LSS and TC forecasts.

With the higher temporal resolution from ABI, the LAP products are now available every 10 min for FD, and every 5 min for CONUS, and every 1 min for the two MESO domains. Forecasters at the HWT have noted and appreciated the increased temporal information from ABI. However, they did raise several limitations that can further improve the usefulness of LAP sounding products. Of all the limitations, the most significant one is probably the clear-sky-only coverage. This is due to the weak penetration capability of IR radiation. Currently, the retrievals are performed only if there are less than 15 cloudy IR pixels with the FOR (a 5 × 5 block). Previous studies (Li et al., 2009; Weisz et al., 2007) have shown that reasonable sounding retrievals could be obtained in certain cloudy conditions, such as thin clouds or low clouds. For area without retrievals (i.e., thick clouds and failed retrievals), NWP forecast profiles can be modified and filled to generate an all sky sounding products. Such products have been developed at Cooperative Institute for Meteorological Satellite Studies and are ready to transition for operational use.

HWT experiments with GOES sounding products have shown that the three LPWs are highly useful and under-utilized for forecasters. The LPW is integrated from the moisture sounding profile for three layers in sigma coordinate: surface–0.9, 0.9–0.7, and 0.7–0.3. It provides forecasters moisture information in lower, middle, and upper troposphere. Seeing differential moisture advection adds significant context to the forecast process. It was particularly useful on days when we had strong low-level moisture advection, tracking the movement of moisture, and dry air aloft. Since its debut in 2016 HWT Spring Experiments, LPW has soon become the favorite LAP product for many forecasters.

To reduce the computation, the GOES-16 LAP products have a spatial resolution of 10 km (i.e., a FOR has 5 × 5 pixels), although ABI IR bands have a spatial resolution of 2 km. This resolution is similar as the previous GOES sounding products. However, refining the resolution to native 2 km would enable forecasters with capability to look into finer details of the moisture and instability field, which could benefit the short-term forecasting and nowcasting of severe storms.

In 2006, the Hyperspectral Environmental Suite was withdrawn from the GOES-R series due to budget constraints. However, NOAA continues to have valid requirement for measurements from an advanced IR sounder in geostationary orbit (Schmit et al., 2009; Wang et al., 2007). In Europe, an advanced IR sounder called InfraRed Sounder has been planned for European Organisation for the Exploitation of Meteorological Satellites Meteosat Third Generation sounding mission to be launched in 2023 time frame. The first

geostationary satellite-based high spectral resolution IR sounder, the Geostationary Interferometric Infrared Sounder onboard FengYun-4A, the first of the Chinese FengYun-4 (FY-4) series (Yang et al., 2017), was launched on 11 December 2016. Compared with traditional GOES sounders, geostationary hyperspectral IR sounders will greatly improve the vertical resolving power, providing more vertical details in atmospheric profiles. Recent Observing System Simulation Study by Li et al. (2018) showed that radiance measurements from a geostationary hyperspectral IR sounder may substantially reduce the overall analysis/forecast when assimilated into NWP models. The ABI LAP will be used before geostationary advanced IR sounder data are available.

References

Bessho, K., Date, K., Hayashi, M., Ikeda, A., Imai, T., Inoue, H., et al. (2016). An introduction to Himawari-8/9—Japan's new-generation geostationary meteorological satellites. *Journal of the Meteorological Society of Japan*, *94*(2), 151–183. https://doi.org/10.2151/jmsj.2016-009

Birkenheuer, D. L., & Gutman, S. I. (2005). A comparison of GOES moisture-derived product and GPS-IPW data during IHOP-2002. *Journal of Atmospheric and Oceanic Technology*, *22*(11), 1838–1845. https://doi.org/10.1175/JTECH1814.1

Borbas, E. E., Seemann, S. W., Huang, H.-L., Li, J., & Menzel, W. P. (2005). *Global profile training database for satellite regression retrievals with estimates of skin temperature and emissivity*, in Proc. Int. ATOVS Study Conf. 14, Bejiing, China.

Chang, P. S., Jelenak, Z., & Alsweiss, S. (2015). Algorithm theoretical basis document: GCOM-W1/AMSR2 Day-1 EDR. Version 2.0, NOAA, March 2015.

Durre, I., Vose, R. S., & Wuertz, D. B. (2006). Overview of the integrated global radiosonde archive. *Journal of Climate*, *19*(1), 53–68. https://doi.org/10.1175/JCLI3594.1

Eyre, J. R., Kelly, G. A., McNally, A. P., Andersson, E., & Persson, A. (1993). Assimilation of TOVS radiance information through one-dimensional variational analysis. *Quarterly Journal of the Royal Meteorological Society*, *119*(514), 1427–1463. https://doi.org/10.1002/qj.49711951411

Galway, J. G. (1956). The lifted index as a predictor of latent instability. *Bulletin of the American Meteorological Society*, *37*(10), 528–529. https://doi.org/10.1175/1520-0477-37.10.528

Jin, X., Li, J., Schmit, T. J., Li, J., Goldberg, M. D., & Gurka, J. J. (2008). Retrieving clear-sky atmospheric parameters from SEVIRI and ABI infrared radiances. *Journal of Geophysical Research*, *113*, D15310. https://doi.org/10.1029/2008JD010040

Lee, Y.-K., Li, J., Li, Z., & Schmit, T. J. (2017). Atmospheric temporal variations in the pre-landfall environment of Typhoon Nangka (2015) observed by the Himawari-8 AHI. *Asia-Pacific Journal of Atmospheric Sciences*, *53*(4), 431–443. https://doi.org/10.1007/s13143-017-0046-z

Lee, Y.-K., Li, Z., Li, J., & Schmit, T. J. (2014). Evaluation of the GOES-R ABI LAP retrieval algorithm using GOES-13 Sounder. *Journal of Atmospheric and Oceanic Technology*, *31*(1), 3–19. https://doi.org/10.1175/JTECH-D-13-00028.1

Li, J., & Huang, H.-L. (1999). Retrieval of atmospheric profiles from satellite sounder measurements by use of the discrepancy principle. *Applied Optics*, *38*(6), 916–923. https://doi.org/10.1364/AO.38.000916

Li, J., Schmit, T. J., Jin, X., & Martin, G. (2012). GOES-R Advanced Baseline Imager (ABI) algorithm theoretical basis document for legacy atmospheric moisture profile, legacy atmospheric temperature profile, total precipitable water, and derived atmospheric stability indices, NOAA NESDIS Center for Satellite Applications and Research Rep. Retrieved from https://www.star.nesdis.noaa.gov/goesr/docs/ATBD/LAP.pdf

Li, J., Wolf, W., Menzel, W. P., Zhang, W., Huang, H.-L., & Achtor, T. H. (2000). Global soundings of the atmosphere from ATOVS measurements: The algorithm and validation. *Journal of Applied Meteorology and Climatology*, *39*(8), 1248–1268.

Li, Z., Li, J., Wang, P., Lim, A., Li, J., Schmit, T. J., Atlas, R., et al. (2018). Value-added impact of geostationary hyperspectral infrared sounders on local severe storm forecasts—Via a quick regional OSSE. *Advances in Atmospheric Sciences*, *35*(10), 1217–1230. https://doi.org/10.1007/s00376-018-8036-3

Li, Z., Li, J., Menzel, W. P., Nelson, J. P. III, Schmit, T. J., Weisz, E., & Ackerman, S. A. (2009). Forecasting and nowcasting improvement in cloudy regions with high temporal GOES sounder infrared radiance measurements. *Journal of Geophysical Research*, *114*, D09216. https://doi.org/10.1029/2008JD010596

Li, Z., Li, J., Menzel, W. P., Schmit, T. J., Nelson, J. P. III, Daniels, J., & Ackerman, S. A. (2008). GOES sounding improvement and applications to severe storm nowcasting. *Geophysical Research Letters*, *35*, L03806. https://doi.org/10.1029/2007GL032797

Lu, J., Feng, T., Li, J., Cai, Z., Xu, X., Li, L., & Li, J. (2019). Impact of assimilating Himawari-8-derived layered precipitable water with varying cumulus and microphysics parameterization schemes on the simulation of Typhoon Hato. *Journal of Geophysical Research: Atmospheres*, *124*, 3050–3071. https://doi.org/10.1029/2018JD029364

Ma, X. L., Schmit, T. J., & Smith, W. L. (1999). A non-linear physical retrieval algorithm—Its application to the GOES-8/9 sounder. *Journal of Applied Meteorology*, *38*(5), 501–513.

Menzel, W. P., Holt, F. C., Schmit, T. J., Aune, R. M., Schreiner, T. J., Wade, G. S., & Gray, D. (1998). Application of GOES-8/9 soundings to weather forecasting and nowcasting. *Bulletin of the American Meteorological Society*, *79*(10), 2059–2077.

Menzel, W. P., & Purdom, J. F. W. (1994). Introducing GOES-I: The first of a new generation of Geostationary Operational Environmental Satellites. *Bulletin of the American Meteorological Society*, *75*(5), 757–781.

Menzel, W. P., Schmit, T. J., Zhang, P., & Li, J. (2018). Satellite-based atmospheric infrared sounder development and applications. *Bulletin of the American Meteorological Society*, *99*(3), 583–603. https://doi.org/10.1175/BAMS-D-16-0293.1

Petty, G. W. (2008). *A First Course in Atmospheric Thermodynamics* (p. 337). Sundog Publishing.

Rocken, C., Vanhove, T., & Ware, R. (1997). Near real-time sensing of atmospheric water vapor. *Geophysical Research Letters*, *24*(24), 3221–3224. https://doi.org/10.1029/97GL03312

Rodgers, C. D. (1976). Retrieval of atmospheric temperature and composition from remote measurements of thermal radiation. *Reviews of Geophysics*, *14*(4), 609–624. https://doi.org/10.1029/RG014i004p00609

Rodgers, C. D. (1990). Characterization and error analysis of profiles retrieved from remote sounding measurements. *Journal of Geophysical Research*, *95*(D5), 5587–5595. https://doi.org/10.1029/JD095iD05p05587

Schmit, T. J., Griffith, P., Gunshor, M. M., Daniels, J. M., Goodman, S. J., & Lebair, W. J. (2017). A closer look at the ABI on the GOES-R series. *Bulletin of the American Meteorological Society*, *98*(4), 681–698. https://doi.org/10.1175/BAMS-D-15-00230.1

Schmit, T. J., Gunshor, M. M., Paul Menzel, W., Gurka, J., Li, J., & Bachmeier, S. (2005). Introducing the next-generation advanced baseline imager (ABI) on GOES-R. *Bulletin of the American Meteorological Society*, *86*(8), 1079–1096. https://doi.org/10.1175/BAMS-86-8-1079

Schmit, T. J., Li, J., Ackerman, S. A., & Gurka, J. J. (2009). High-spectral- and high-temporal-resolution infrared measurements from geostationary orbit. *Journal of Atmospheric and Oceanic Technology*, *26*(11), 2273–2292. https://doi.org/10.1175/2009JTECHA1248.1

Schmit, T. J., Li, J., Gurka, J. J., Goldberg, M. D., Schrab, K., Li, J., & Feltz, W. (2008). The GOES-R Advanced Baseline Imager and the continuation of current GOES sounder products. *Journal of Applied Meteorology and Climatology*, *47*(10), 2696–2711. https://doi.org/10.1175/2008JAMC1858.1

Seemann, S. W., Borbas, E. E., Knuteson, R. O., Stephenson, G. R., & Huang, H.-L. (2008). Development of a global infrared land surface emissivity database for application to clear sky sounding retrievals from multi-spectral satellite radiance measurements. *Journal of Applied Meteorology and Climatology*, *47*(1), 108–123. https://doi.org/10.1175/2007JAMC1590.1

Seemann, S. W., Li, J., Menzel, W. P., & Gumley, L. E. (2003). Operational retrieval of atmospheric temperature, moisture, and ozone from MODIS infrared radiances. *Journal of Applied Meteorology and Climatology*, *42*(8), 1072–1091. https://doi.org/10.1117/12.466686

Smith, W. L., & Woolf, H. M. (1976). The use of eigenvectors of statistical covariance matrices for interpreting satellite sounding radiometer observations. *Journal of the Atmospheric Sciences*, *33*(7), 1127–1140.

Sun, B., Reale, A., Tilley, F. H., Pettey, M. E., Nalli, N. R., & Barnet, C. D. (2017). Assessment of NUCAPS S-NPP CrIS/ATMS sounding products using reference and conventional radiosonde observations. *IEEE Journal of Selected Topics in Applied Earth Observations and Remote Sensing*, *10*(6), 2499–2509. https://doi.org/10.1109/JSTARS.2017.2670504

Turner, D. D., Lesht, B. M., Clough, S. A., Liljegren, J. C., Revercomb, H. E., & Tobin, D. C. (2003). Dry bias and variability in Vaisala RS80-H radiosondes: The ARM experience. *Journal of Atmospheric and Oceanic Technology*, *20*(1), 117–132. https://doi.org/10.1175/1520-0426(2003)020<0117:DBAVIV>2.0.CO;2

Turner, D. D., & Lohnert, U. (2014). Information content and uncertainties in thermodynamic profiles and liquid cloud properties retrieved from the ground-based Atmospheric Emitted Radiance Interferometer (AERI). *Journal of Applied Meteorology and Climatology*, *53*(3), 752–771. https://doi.org/10.1175/JAMC-D-13-0126.1

Wang, F., Li, J., Schmit, T. J., & Ackerman, S. A. (2007). Trade studies of hyperspectral infrared sounder on geostationary satellite. *Applied Optics*, *46*(2), 200–209. https://doi.org/10.1364/AO.46.000200

Wang, P., Li, J., Lu, B., Schmit, T. J., Lu, J., Lee, Y.-K., et al. (2018). Impact of moisture information from Advanced Himawari Imager measurements on heavy precipitation forecasts in a regional NWP model. *Journal of Geophysical Research: Atmospheres*, *123*, 6022–6038. https://doi.org/10.1029/2017JD028012

Ware, R. H., Fulker, D. W., Stein, S. A., Anderson, D. N., Avery, S. K., Clark, R. D., et al. (2000). Suominet: A real-time national GPS network for atmospheric research and education. *Bulletin of the American Meteorological Society*, *81*(4), 677–694.

Weisz, E., Li, J., Li, J., Zhou, D. K., Huang, H.-L., Goldberg, M. D., & Yang, P. (2007). Cloudy sounding and cloud-top height retrieval from AIRS alone single field-of-view radiance measurements. *Geophysical Research Letters*, *34*, L12802. https://doi.org/10.1029/2007GL030219

Xie, H., Nalli, N. R., Sampson, S., Wolf, W. W., Li, J., Schmit, T. J., et al. (2013). Integration and ocean-based prelaunch validation of GOES-R Advanced Baseline Imager legacy atmospheric products. *Journal of Atmospheric and Oceanic Technology*, *30*(8), 1743–1756. https://doi.org/10.1175/JTECH-D-12-00120.1

Yang, Y., Moore, S., Uddstrom, M., Turner, R., & Carey-Smith, T. (2017). Model moist bias in the middle and upper troposphere during DEEPWAVE. *Atmospheric Science Letters*, *18*(4), 161–167. https://doi.org/10.1002/asl.738